NÖHÜ Müh. Bilim. Derg. / NOHU J. Eng. Sci., 2023; 12(3), 998-1006

Niğde Ömer Halisdemir Üniversitesi Mühendislik Bilimleri Dergisi
Niğde Ömer Halisdemir University Journal of Engineering Sciences

Araştırma makalesi / Research article

www.dergipark.org.tr/tr/pub/ngumuh / www.dergipark.org.tr/en/pub/ngumuh

Degradation of methylene blue and rhodamine B by hollow ZnO microspheres formed of radially oriented nanorods

Metilen mavisi ve rhodamine B'nin radyal olarak yönlendirilmiş ZnO nanoçubuklardan oluşan içi boş mikroküreler tarafından bozunması

Hasan Eskalen[1], Mustafa Kavgacı[2*]

[1] *Kahramanmaraş Sütçü İmam University, Vocational School of Health Services, Department of Opticianry, 46100, Kahramanmaraş, Türkiye*
[2] *Kahramanmaraş İstiklal University, Elbistan Vocational School of Health Services, Department of Opticianry, 46300, Kahramanmaraş, Türkiye*
[1,2] *Kahramanmaraş Sütçü İmam University, Graduate School of Natural and Applied Sciences, Department of Material Science and Engineering, 46050, Kahramanmaraş, Türkiye*

Abstract

It is crucial to find effective solutions to environmental contamination that are also ecologically friendly. Zinc oxide (ZnO) is well-known as a promising photocatalyst. In this work, ZnO microspheres were synthesized using the solvothermal technique. X-ray diffraction (XRD), UV-Vis, and scanning electron microscopy (SEM) were used to evaluate the structural, optical, and morphological features of ZnO microspheres. The hexagonal structure of ZnO was determined using XRD analysis. The crystal size of ZnO was calculated using XRD patterns and was found to be 44.27 nm by the Debye-Scherrer equation, 32.39 nm by using the Williamson Hall model, and 9.92 nm by the Modified Scherrer formula. The SEM pictures of the manufactured ZnO revealed that it has a shape in the form of microspheres formed by the conjunction of hexagonal nanorods. The average diameter of these microspheres is 5.16 µm. ZnO has a band gap energy of 3.1 eV. The photocatalytic activities of ZnO microspheres against methylene blue and Rhodamine B dyes were examined. Under sunlight, photocatalytic removal rates for methylene blue after 90 minutes and Rhodamine B after 120 minutes were 98.95% and 98.62%, respectively.

Keywords: ZnO, Microspheres, Methylene blue, Rhodamine B, Photocatalytic

Öz

Çevre kirliliğine karşı çevre dostu etkili çözümler bulmak çok önemlidir. Çinko oksit (ZnO), iyi bir fotokatalizör olarak bilinir. Bu çalışmada solvotermal teknik kullanılarak ZnO mikroküreler sentezlenmiştir. ZnO mikrokürelerin yapısal, optik ve morfolojik özelliklerini değerlendirmek için X-ışını kırınımı (XRD), UV-Vis ve taramalı elektron mikroskobu (SEM) kullanıldı. ZnO'nun hegzagonal yapısı, XRD analiziyle belirlendi. ZnO'nun kristal boyutu, XRD desenleri kullanılarak hesaplandı ve Debye-Scherrer denklemi ile 44.27 nm, Williamson Hall modeli kullanılarak 32.39 nm ve Modifiye Scherrer formülü ile 9.92 nm olarak bulundu. Üretilen ZnO'nun SEM görüntüleri, altıgen nanoçubukların birleşmesiyle oluşan mikroküreler şeklinde bir yapıya sahip olduğunu ortaya koydu. Bu mikrokürelerin ortalama çapı 5.16 µm'dir. ZnO, 3.1 eV'lik bir bant aralığı enerjisine sahiptir. ZnO mikrokürelerin metilen mavisi ve Rhodamine B boyalarına karşı fotokatalitik aktiviteleri incelenmiştir. Güneş ışığı altında, 90 dakika sonunda metilen mavisi ve 120 dakika sonra Rhodamine B için fotokatalitik giderme oranları sırasıyla %98.95 ve %98.62'dir.

Anahtar kelimeler: ZnO, Mikroküreler, Metilen mavisi, Rhodamine B, Fotokatalitik

1 Introduction

Water is one of the most critical components for the survival of all living organisms on the earth [1]. Water resource pollution caused by influents from diverse sectors such as textile, paper, leather pharmaceutical, cosmetics and paints a hazard to human health and the ecological system [2–4]. The majority of dyes have complex structures and great chemical stability, which enable them to linger in flowing water for extended periods of time, preventing the growth of aquatic biota by absorbing dissolved oxygen and blocking sun light, and decreasing the recreational value of the stream [5]. Detoxifying such harmful contaminants is crucial for maintaining a clean environment since industrial effluents are released directly into open water systems without adequate treatment, which poses significant risks to the environment [3]. To ensure a nontoxic and pollution-free environment, it has been prioritized to separate and degrade these organic waste products [6,7]. Coagulation, adsorption, flocculation, advanced oxidation, and precipitation are some examples of classic wastewater treatment methods that not only take a long time to complete but also create secondary sludge that is expensive to dispose of. Photocatalytic degradation of organic pollutants has drawn a lot of interest among these various techniques for treating dye-contaminated water [8] due to its cost-effectiveness, reusability, and environmental friendliness [9,10]. With this technique, organic contaminants are broken down or oxidized into less dangerous or non-hazardous compounds [11].

* Sorumlu yazar / Corresponding author, e-posta / e-mail: mkavgaci@gmail.com (M. Kavgacı)
Geliş / Recieved: 28.12.2022 Kabul / Accepted: 16.05.2023 Yayımlanma / Published: 15.07.2023
doi: 10.28948/ngmuh.1225826

For the photodegradation of different organic dyes, several semiconductors such as titanium dioxide, cadmium sulfide, vanadium(V) oxide, tungsten (VI) oxide, copper oxide, and zinc oxide have been employed up to date [12]. Arundo donax L. ash was used for the first time to produce amorphous SiO_2. The increased photocatalytic degradation activity in 50 wt% SiO_2-50 wt% TiO_2 nanocomposite sample was reported due to better light absorption and charge carrier separation by modifying the electronic structure [13]. Inorganic materials' morphologies are acknowledged to significantly impact the vast range of their characteristics and associated potential uses. It is commonly known that among wide-band gap semiconductors, ZnO shows the most variety of morphologies [14]. Moreover, ZnO nanoparticles (NPs) are attractive because of their inexpensive cost, high band gap energy of 3.37 eV, and high exciton binding energy of 60 meV [14,15]. ZnO nanostructures with a unique morphology resembling flowers have received much interest due to their exceptional performance in various fields [16]. Methylene blue (MB) dye was removed using the ZnO-NFs' photocatalytic performance when exposed to sunlight, and 88.39% of the dye was photodegraded in 180 minutes [17]. After a 150 minute photodegradation operation, the MB dye's degradation efficiency of different morphological ZnO was reported as 91% (for the Zn powder source) and 93% (for the Zn sheet source) [18]. After 7 hours of exposure, visible-light photocatalytic activity of MB was reported to be 98% in ZnO particles with a triangular morphology [19]. At 180 minutes, spherical ZnO nanoparticles synthesized with oregano extract degraded Rhodamine B dye by 93% was reported [20].

With the above aforementioned factors, in this study, ZnO nanomaterial in hollow ZnO microspheres composed of radially aligned nanorods morphology was synthesized. The morphology, crystal structure and optical feature of the synthesized photocatalyst was investigated. The novelty of this study is to synthesize the hollow ZnO microspheres composed of radially aligned nanorods through hydrothermal methods. Two dyes methylene blue (MB) and Rhodamine B (RhB) were selected for the photocatalytic reaction performance test and the degradation of these dyes reached to 98.95 and 98.62, respectively. To the present, there is no report in the literature stating this maximum degradation and mineralization of MB and RhB using hollow ZnO microspheres composed of radially aligned nanorod.

2 Materials and method

2.1 Materials

Zinc nitrate hexahydrate ($Zn(NO_3)_2{\cdot}6H_2O$) was purchased from Across organics, ethylene glycol ($(CH_2OH)_2$), ammonium hydroxide ($NH_3{\cdot}H_2O$) and sodium carbonate (Na_2CO_3) from Sigma Aldrich. Methylene Blue was supplied from AFG Bioscience, and Rhodamine B from Isolab. All chemicals utilized in this work were reagent grade and were not purified further.

2.2 Preparation of ZnO nanoparticles

To synthesize ZnO microspheres, 0.1M $Zn(NO_3)_2.6{\cdot}H_2O$ was homogeneously dissolved in 150 mL of ethylene glycol for half an hour on a magnetic stirrer. Dropwise, 9 mL of NH_3H_2O (25-28% wt) was added to this solution. Then 5 mM Na_2CO_3 was dissolved in the resulting mixture to create a homogenous solution. This mixture was put into a teflon container. The teflon container was heated in a steel autoclave for 12 hours at 150 °C. The autoclave was allowed to cool at ambient temperature after heat treatment. The water was then filtered with filter paper. The obtained sample was washed multiple times and dried for three hours at 45 °C. Following this, it was thermally treated for 3 hours in air at 450 °C.

2.3 Characterization

Using an XRD (X-ray diffraction) instrument, the structural characteristics of the generated ZnO microspheres were studied. The XRD patterns were obtained using a Philips X'Pert PRO brand XRD device equipped with Cu Ka radiation. The optical characteristics of the generated ZnO microspheres were examined using a UV-Visible Spectrophotometer (Shimadzu UV 1800). SEM (Scanning Electron Microscopy) pictures of ZnO microspheres were obtained using an FEI Quanta 650 type electron microscope.

2.4 Photocatalytic parameters testing

The photocatalytic activities of two dyes, methylene blue (MB) and rhodamine B (RhB), were examined. As a light source, a 300-watt xenon lamp was utilized. UV-Vis spectroscopy was used to quantify photocatalytic degradation in the 400-750 nm region. Degradation was measured by preparing 50 mL solutions of dyestuffs at 5 ppm (mgL^{-1}). Each experiment utilized 10 mg of manufactured ZnO microspheres. After mixing ZnO with the microspheres dye solutions were held in the dark for 30 minutes to guarantee adsorption-desorption equilibrium. Then, from 0 to 90 minutes for MB and 0 to 120 minutes for RB, 2 ml samples were obtained every 10 minutes, and their measurements were recorded by detecting them in UV-Vis spectroscopy.

The following equation was used to calculate the percent distortions of MB and RB:

$$Degradation\ (\%) = \frac{C_0 - C_t}{C_0} \times 100 \qquad (1)$$

where C_0 is the starting concentration of MB and RB solution (gL^{-1}) at t = 0 min, and C_t is the concentration of MB and RB dye (gL^{-1}) at various intervals.

The Langmuir-Hinshelwood model was used to investigate the kinetics of dye degradation. The L-H model works well for heterogeneous photocatalysis at low dye concentrations, and the equation is as follows.

$$ln(C_t / C_0) = -k{\cdot}t \qquad (2)$$

where C_0 is the dye concentration in solution at time 0, C_t is the dye concentration in solution at time t, k is the rate constant, and t is the reaction time [21,22].

3 Results and discussion

X-ray diffraction was taken to confirm that the produced nanoparticles have the ZnO phase. The XRD pattern of nanoparticles is given in Figure 1. Very strong diffraction peaks were observed in the XRD pattern of the produced ZnO nanoparticles. These peaks correspond to the values of 31.73°, 34.39°, 36.22°, 47.52°, 56.59°, 62.86°, 65.96°, 67.96°, and 69.06° 2θ, respectively, (100), (002), (101), (102), (110), (103), (112) and (201) planes. The XRD diffraction peaks are in good agreement with the literature. All peaks are in agreement with PDF: 01-080-0075 and confirm that the ZnO phase has a hexagonal structure [23].

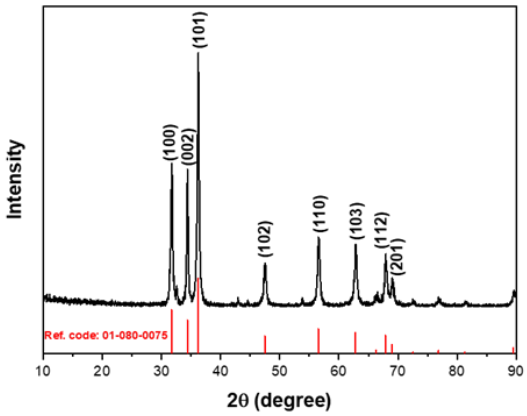

Figure 1. XRD pattern of the ZnO

The particle sizes of produced materials may be examined using XRD patterns. The Debye-Scherrer equation is one of several methods for calculating the size of nanoparticles. Debye-Scherrer equation:

$$D = k\lambda/\beta cos\ \theta \tag{3}$$

The particle size is represented by the letter D in the equation. The wavelength of the incident radiation (λ) is equal to 1,54056 A. The variable k in the equation is a constant number (k=0.94 for CuKa radiation). β denotes the breadth at position of the peak at half-maximum intensity. θ is the angle of diffraction of the peak.

The uniform deformation model (UDM) described by Williamson-Hall can be used to analyze internal tension. UDM may be used to study the samples' internal stress, as suggested by Williamson-Hall. The equation below may be used to determine the expansion brought on by lattice stress, which can result in crystal defects and deformations in materials in powder form:

$$\varepsilon = \frac{\beta_{hkl}}{4\ tan(\theta)} \tag{4}$$

Following are the W-H Equations (5) and (6) that produce the overall expansion:

$$\beta_{hkl} = \frac{K\ \lambda}{D\ cos\theta} + 4\varepsilon\ tan(\theta) \tag{5}$$

Adjusted equation (4):

$$\beta_{hkl}\ cos(\theta) = \frac{K\ \lambda}{D} + 4\varepsilon\ sin(\theta) \tag{6}$$

The least square mean of all the peaks may be used to estimate the D value pretty precisely using the modified Scherer formula. Its formula is as follows:

$$\beta = k\lambda/Dcos\ \theta\ =\ (k\lambda/D)(1/cos\theta) \tag{7}$$

If you take the logarithm of both sides of the equation [24–26]:

$$ln\ \beta = ln(k\lambda/D) +\ ln(1/cos\theta) \tag{8}$$

The size of the particles is an important parameter. In order to evaluate the particle sizes of the ZnO nanoparticles produced in the study, it was calculated using the Debye-Scherrer, Williamson-Hall and Modified Scherrer equations. The plot is drawn with cos(θ) on the y-axis and 1/β on the x-axis, as shown in Figure 2a. The dimensions of the produced ZnO nanoparticles were calculated using the Debye-Scherrer equation and the dimensions of the particles were found to be 44.273 nm. The crystal sizes of ZnO nanoparticles can be examined in more detail by using the Williamson-Hall plot. Williamson Hall graph is given in Figure 2b. It is seen that the graph has a linear relationship and a positive slope. The effective particle size for ZnO nanoparticles was calculated as 32.39 nm by the Williamson-Hall equation. Using the slope of the graph where ln(1/cosθ) is the x-axis and lnβ is the y-axis, the dimensions of ZnO nanoparticles were estimated as 9.92 nm from the Modified Scherrer formula.

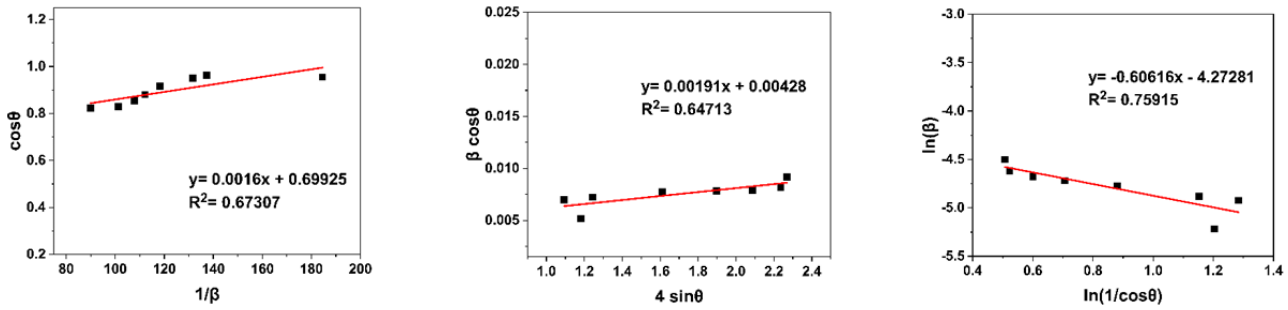

(a) (b) (c)

Figure 2. The plot of Debye Sherrer (a) WH (b) Modified Schere (c)

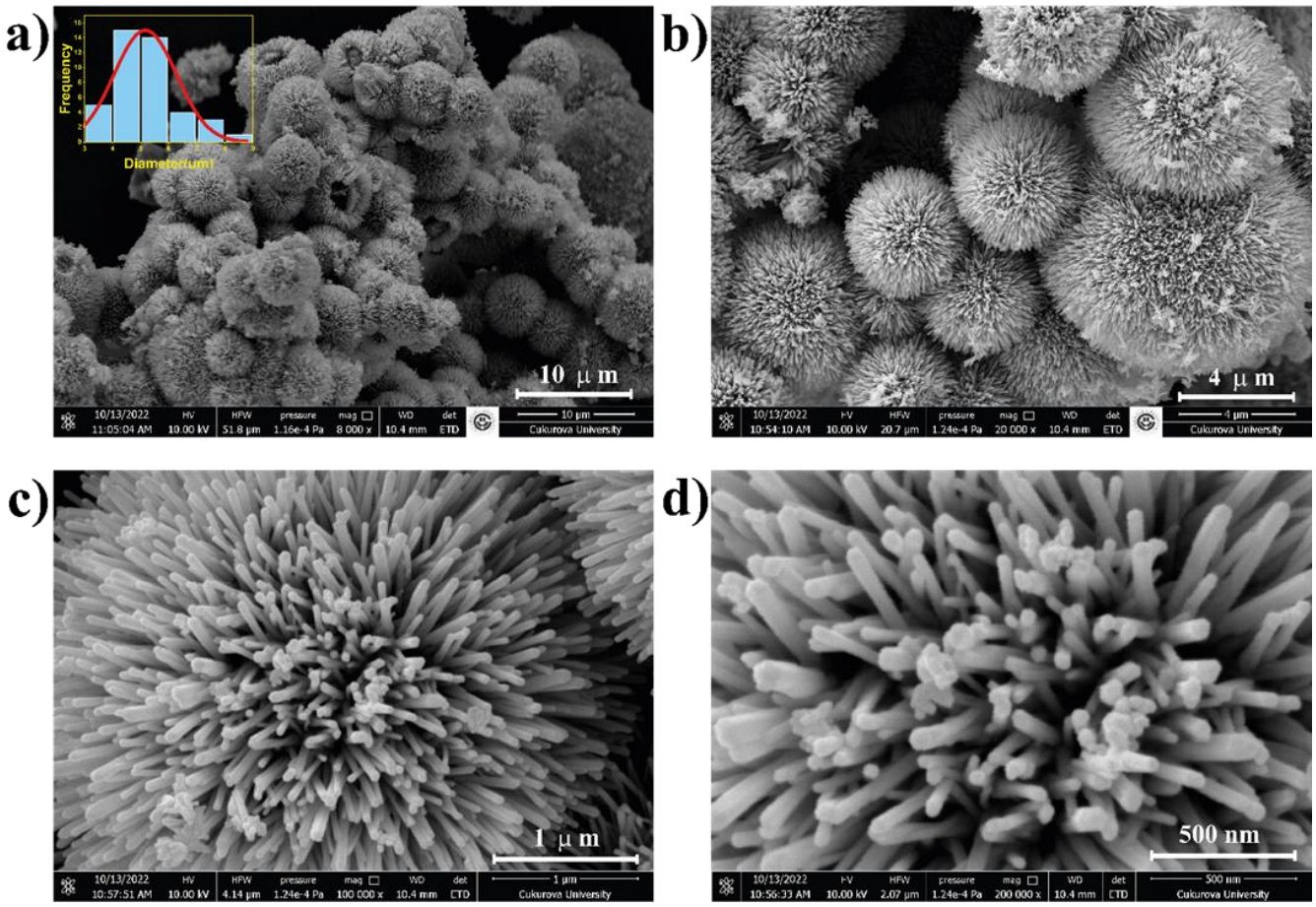

Figure 3. SEM images of ZnO at low magnification (a-b) and high magnification (c–d)

The morphological properties of the produced ZnO nanoparticles were characterized by SEM and the obtained images are presented in Figure 3. As can be seen from the SEM images, ZnO has a uniform morphology in the form of microspheres formed by the combination of hexagonal nanorods. The visible ZnO microspheres have diameters in the 3–9 µm range. The mean diameter of these microspheres is 5.16 µm. In Figures 3c and 3d, it can be clearly seen that the morphology of ZnO consists of nano-sized hexagonal rod structures [27]. The hexagonal structure seen here is consistent with the XRD results.

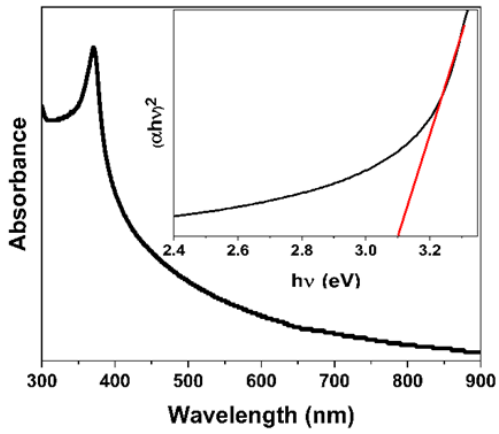

Figure 4. Absorbance and bandgap pattern of ZnO

The optical properties of ZnO microspheres were investigated by UV-vis and the spectra in the 300–900 nm range are shown in Figure 4. When the absorption spectrum of ZnO microspheres is examined, it has a strong absorption in the wavelength range of 350-400 nm in the UV region. This absorption peak peaked at about 371 nm. This result indicates that the ZnO sample can be excited by ultraviolet and visible light sources. The band gap energies of the synthesized ZnO microspheres can be obtained by the Tauc method by utilizing the $(\alpha h\nu)^2$ versus $(h\nu)$ plot. In this way, the band gap energies of ZnO microspheres were estimated as 3.1 eV. This result is compatible with the literature [28–30].

Photocatalytic degradation of MB dye under sunlight simulator illumination in the presence of produced ZnO microspheres is shown in Figure 5. When the UV-Vis absorption spectra for the MB dye were examined, the maximum absorbance was found at 664 nm. For MB, the absorption gradually decreased steadily with increasing illumination time. The UV absorption peaks for MB were reduced to almost zero after 90 minutes under sunlight.

In Figure 6, the degradation of ZnO microspheres on MB dyestuff after 90 minutes was determined to be approximately 98.95%. The degradation rate of the dyestuff under sunlight without a photocatalyst is 1.82%.

The rate of decay MB for ZnO microspheres is shown in Figure 7a and 7b. The decay rate constant k under the

illumination of solar simulator light was evaluated by plotting a graph of $\ln(C_t/C_0)$ against the illumination time (t) (Figure 7). To calculate the k value, a pseudo-first-order model was employed. Figure 7b makes it evident that time and $\ln(C_t/C_0)$ have a strong longitudinal reliance on ZnO microspheres. ZnO microspheres MB decay k-value was calculated to be 0.05175 min^{-1}.

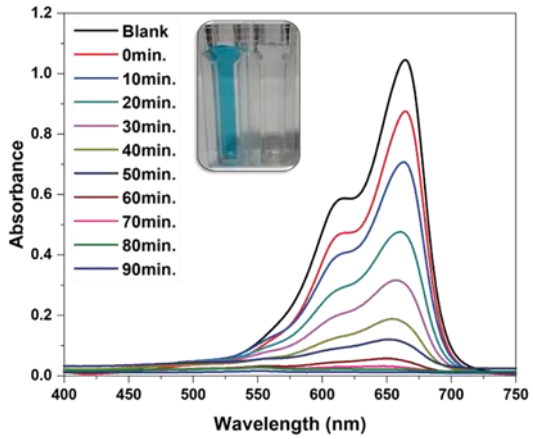

Figure 5. UV-visible absorption spectra of MB in the presence of ZnO microspheres over time

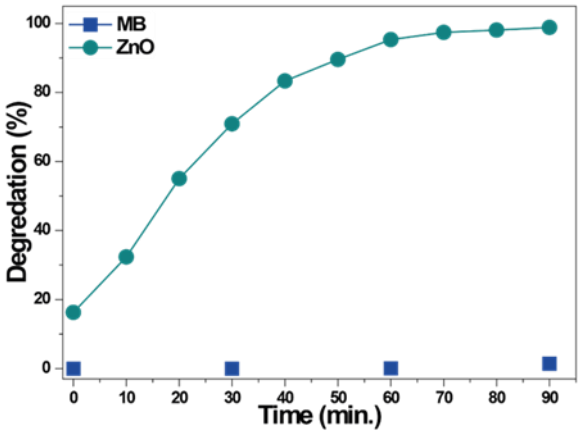

Figure 6. Photocatalytic degradation of MB in the presence and scarcity of ZnO

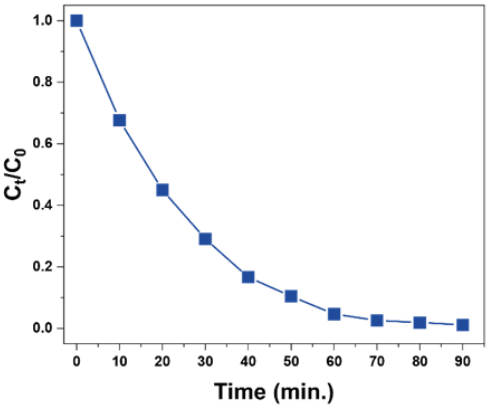

(a)

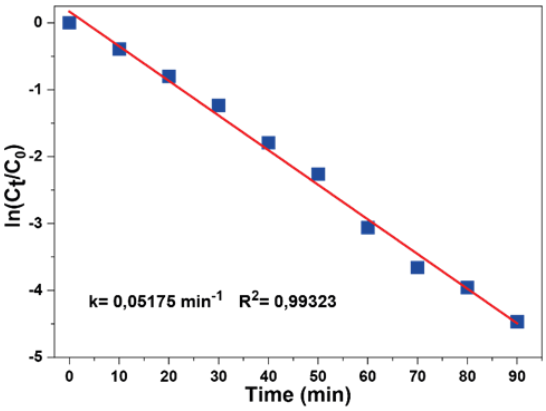

(b)

Figure 7. Concentration ratio (C_t/C_o) vs time plot (a) Dye degradation $\ln(C_t/C_o)$ against time spectrum (b)

The time-dependent photocatalytic degradation of ZnO microspheres RB in solar simulator illumination was investigated. RB degradation was determined by recording the absorbance decreases with the maximum peak in the UV-Vis absorption spectrum at 554 nm. The absorbance graph of RB is given in Figure 8. In the solar simulator light, the absorption peaks for RB approached nearly zero at the end of 120 minutes.

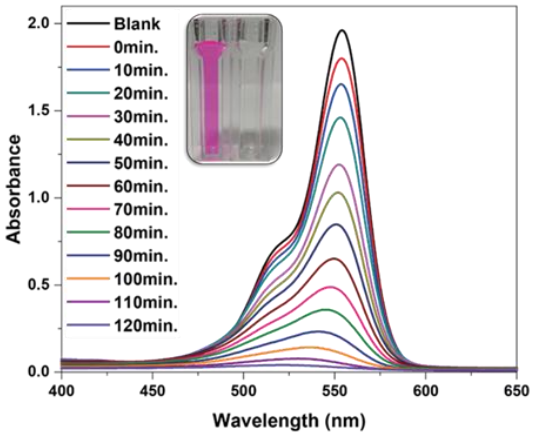

Figure 8. UV-visible absorption spectra of RB in the presence of ZnO microspheres over time

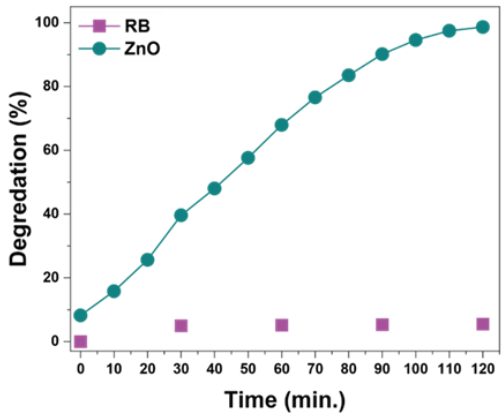

Figure 9. Photocatalytic degradation of RB in the presence and scarcity of ZnO

After 120 min, the degradation of the ZnO photocatalyst on RB was 98.62%. The self-degradation rate of RB dyestuff was found to be 5.5% under solar simulator light without ZnO microspheres.

Figures 10a and 10b show graphs of the degradation rate of the generated ZnO samples on RB. Using the pseudo-first-order model, the decay rate value k was computed as a 0.03405 min^{-1}.

The photocatalytic activity of freshly synthesized hollow microspheres with radially aligned nanorod ZnO and various morphologies ZnO nanoparticles is presented in Table 1.

Because of its low cost and non-toxicity, ZnO is frequently utilized as an excellent photocatalyst for the breakdown of dyes. Figure 11 schematically illustrates a proposed photodegradation mechanism of MB and RB by ZnO microspheres under sunlight. It is fair to speculate that ZnO's improved photocatalytic characteristics are owing to its huge surface area, more oxygen vacancies, and higher charge separation and transfer efficiencies. In the photocatalytic process, MB or RB molecules are adsorbed on the surface of ZnO microspheres. Under sunlight, MB or RB dye radicals are generated. Similarly, electron-hole (e^--h^+) pairs may be formed in ZnO microspheres when exposed to sunshine. These electron-hole pairs can be removed from the ZnO surface. Following this, superoxide anion ($\cdot O_2^-$) can be generated as a result of the interaction of electrons (e^-) with oxygen molecules (O_2). The interaction of these superoxide anions with H^+ can produce hydroxyl radical (·OH). Holes (h^+) may oxidize water molecules (H_2O) and hydroxyl ions (OH^-) to generate a hydroxyl radical (·OH). The O_2 and OH radicals are very reactive and can oxidize and damage MB or RB [27,38–41].

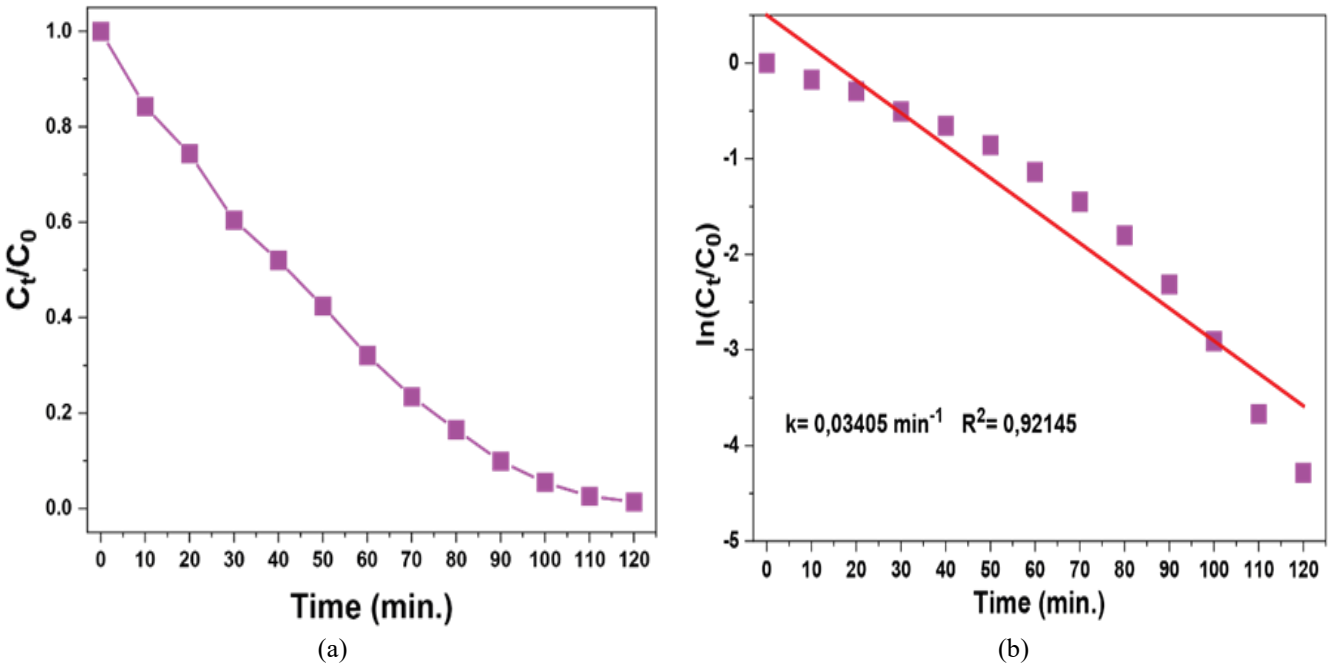

(a) (b)

Figure 10. Concentration ratio (C_t/C_o) vs time plot (a) Dye degradation ln(C_t/C_o) against time spectrum (b)

Table 1. Comparison study of degradation for different morphological ZnO nanoparticles

Morphology of Photocatalyst and concentration	Dye and dye Concentration	Type of Irradiation	Irradiation Time (min)	% Degradation	Ref.
Spherical ZnO (50 mg)	RhB (15 ppm)	UV-light Solar light	100 min 180 min	94.24 93	[20]
Disk like ZnO/nanocellulose (35 mg)	MB (3.25 g/L)	UV-light	300 min	79	[31]
Finger-like macro-voids ZnO/cellulose acetate (10 mg)	MB (100 ppm)	UV-light Solar light	120 min 120 min	30 75	[32]
Oval-shaped ZnO (50 mg)	MB (10 mg/L)	UV-light	180 min	54	[33]
Cauliflower-like ZnO (20 mg)	MB (2.24 µM)	UV-light	180 min	88.2	[34]
Flowerlike ZnO (20 mg)	RhB (10 µM)	Solar light	200 min	98	[35]
Cube like ZnO (0.8 g/L)	RhB (20 mg/L)	Solar light	240 min	71	[36]
Spherical like ZnO (100 mg)	RhB (10 ppm)	Solar light	300 min	80.13	[37]
Microspheres formed of radially oriented nanorods ZnO (10 mg)	MB (5 ppm) RhB (5 ppm)	Solar light Solar light	90 min 120 min	98.95 98.62	This work

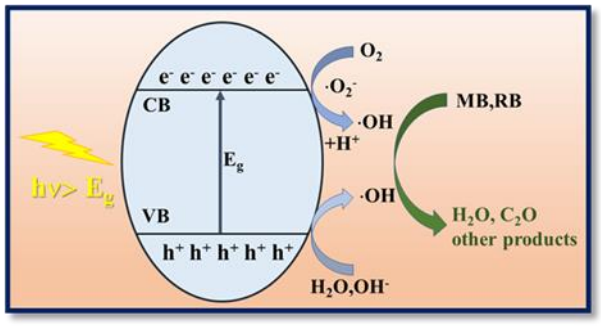

Figure 21. The photocatalytic mechanism of MB and RB degradation in a ZnO sample [42]

4 Conclusion

The hydrothermal process was used to synthesize ZnO microspheres. In ZnO microspheres, the crystal structure was found as hexagonal. The mean sphere diameter of the ZnO microspheres was 5.16 m, while their sizes ranged from 3 to 9 m. The synthesized ZnO microspheres imply that electron-hole pairs may be effectively separated and transported. Therefore, it is logical to hypothesize that the effective photocatalytic qualities may be brought about by a more significant surface area, more oxygen vacancies, and higher charge separation and transfer efficiency. The ability to exploit ambient sunlight was detected in the synthesized microspheres, which were highly effective photocatalysts with wide-bandgap energy. The created microspheres show promise and may be applied in photocatalytic processes that utilize sunlight to remediate wastewater.

Acknowledgment

This study was supported by the Scientific Research Projects Coordination Unit of Kahramanmaraş Sütçü İmam University. Project number 2020/3-7 YLS, 2022/6-4 YLS.

Conflict of interest

The authors declare that there is no conflict of interest.

Similarity rate (iThenticate): %16

References

[1] M. Binsabt, V. Sagar, J. Singh, M. Rawat and M. Shaban, Green Synthesis of CS-TiO_2 NPs for Efficient Photocatalytic Degradation of Methylene Blue Dye. Polymers, 14, 2677, 2022. https://doi.org/10.3390/polym14132677.

[2] N. Madima, K.K. Kefeni, S.B. Mishra, A.K. Mishra and A.T. Kuvarega, Fabrication of magnetic recoverable Fe_3O_4/TiO_2 heterostructure for photocatalytic degradation of rhodamine B dye. Inorganic Chemistry Communications, 145, 109966, 2022. https://doi.org/10.1016/j.inoche.2022.109966.

[3] Y. Yang, H. Khan, S. Gao, A.K. Khalil, N. Ali, A. Khan, P.L. Show, M. Bilal and H. Khan, Fabrication, characterization, and photocatalytic degradation potential of chitosan-conjugated manganese magnetic nano-biocomposite for emerging dye pollutants. Chemosphere, 306, 135647, 2022. https://doi.org/10.1016/j.chemosphere.2022.135647.

[4] G.D. Okçu, H.E. Ökten and A. Yalçuk, The review study on removal of pesticides in photocatalysis and biological treatment hybrid process. Niğde Ömer Halisdemir University Journal of Engineering Sciences, 8, 675–688, 2019. https://doi.org/10.28948/ngumuh.598101.

[5] S. Sugashini, T. Gomathi, R.A. Devi, P.N. Sudha, K. Rambabu and F. Banat, Nanochitosan/carboxymethyl cellulose/TiO_2 biocomposite for visible-light-induced photocatalytic degradation of crystal violet dye. Environmental Research, 204, 112047, 2022. https://doi.org/10.1016/j.envres.2021.112047.

[6] N. Qutub, P. Singh, S. Sabir, S. Sagadevan and W.C. Oh, Enhanced photocatalytic degradation of Acid Blue dye using CdS/TiO_2 nanocomposite. Scientific Reports, 12:1, 5759, 2022. https://doi.org/10.1038/s41598-022-09479-0.

[7] C.B. Özkal and S.M. Pagano, Evaluation of antibiotics and antibiotic resistant bacteria removal by photo-catalysis. Niğde Ömer Halisdemir University Journal of Engineering Sciences, 5, 1–18, 2016.

[8] S.A. Kumar, M. Jarvin, S.S.R. Inbanathan, A. Umar, N.P. Lalla, N.Y. Dzade, H. Algadi, Q.I. Rahman and S. Baskoutas, Facile green synthesis of magnesium oxide nanoparticles using tea (Camellia sinensis) extract for efficient photocatalytic degradation of methylene blue dye. Environmental Technology Innovation, 28, 102746, 2022. https://doi.org/10.1016/j.eti.2022.102746.

[9] A. Zia, A.B. Naveed, A. Javaid, M.F. Ehsan and A. Mahmood, Facile Synthesis of ZnSe/Co_3O_4 Heterostructure Nanocomposites for the Photocatalytic Degradation of Congo Red Dye. Catalysts, 2, 1184, 2022. https://doi.org/10.3390/catal12101184.

[10] S.Ü. Odabaşı, S.H. Altin and H. Büyükgüngör, Occurence, fate and removal of micropollutants from aquatic environment with advanced oxidation processes. Niğde Ömer Halisdemir University Journal of Engineering Sciences, 9, 57–71, 2020. https://doi.org/10.28948/ngumuh.526064.

[11] K. Arya, A. Kumar, A. Sharma, S. Singh, S.K. Sharma, S.K. Mehta and R. Kataria, A Hybrid Nanocomposite of Coordination Polymer and rGO for Photocatalytic Degradation of Safranin-O Dye Under Visible Light Irradiation. Topics in Catalysis, 65, 1924–1937, 2022. https://doi.org/10.1007/S11244-022-01701-7.

[12] A. M. Naji, I. Y. Mohammed, S.H. Mohammed, M.K.A. Mohammed, D.S. Ahmed, M.S. Jabir and A. M. Rheima, Photocatalytic degradation of methylene blue dye using F doped ZnO/polyvinyl alcohol nanocomposites. Materials Letters, 322, 132473, 2022. https://doi.org/10.1016/j.matlet.2022.132473.

[13] G. Easwaran, J.S. Packialakshmi, A. Syed, A.M. Elgorban, M. Vijayan, K. Sivakumar, K. Bhuvaneswari, G. Palanisamy and J. Lee, Silica nanoparticles derived from Arundo donax L. ash composite with Titanium dioxide nanoparticles as an efficient nanocomposite for photocatalytic degradation

dye. Chemosphere, 307, 135951, 2022. https://doi.org/10.1016/j.chemosphere.2022.135951.

[14] Y. Wang, X. Li, N. Wang, X. Quan and Y. Chen, Controllable synthesis of ZnO nanoflowers and their morphology-dependent photocatalytic activities. Separation and Purification Technology, 62, 727–732, 2008. https://doi.org/10.1016/j.seppur.2008.03.035.

[15] H. Eskalen, Ş. Özğan, Ü. Alver and S. Kerli, Electro-optical properties of liquid crystals composite with zinc oxide nanoparticles. Acta Physica Polonica A, 127, 756–760, 2015. https://doi.org/10.12693/aphyspola.127.756.

[16] A. Das, P. M. Kumar, M. Bhagavathiachari and R.G. Nair, Shape selective flower-like ZnO nanostructures prepared via structure-directing reagent free methods for efficient photocatalytic performance. Materials Science and Engineering: B, 269, 115149, 2021. https://doi.org/10.1016/j.mseb.2021.115149.

[17] R. Vinayagam, S. Pai, T. Varadavenkatesan, A. Pugazhendhi and R. Selvaraj, Characterization and photocatalytic activity of ZnO nanoflowers synthesized using Bridelia retusa leaf extract. Applied Nanoscience, 1, 1–10, 2021.https://doi.org/10.1007/S13204-021-01816-5.

[18] A. Mohammadzadeh, M. Khoshghadam-Pireyousefan, B. Shokrianfard-Ravasjan, M. Azadbeh, H. Rashedi, M. Dibazar and A. Mostafaei, Synergetic photocatalytic effect of high purity ZnO pod shaped nanostructures with H_2O_2 on methylene blue dye degradation. Journal Alloys and Compounds, 845, 156333, 2020. https://doi.org/10.1016/j.jallcom.2020.156333.

[19] F.H. Abdullah, N.H.H. Abu Bakar and M. Abu Bakar, Low temperature biosynthesis of crystalline zinc oxide nanoparticles from Musa acuminata peel extract for visible-light degradation of methylene blue. Optik, 206, 164279, 2020. https://doi.org/10.1016/j.ijleo.2020.164279.

[20] P.A. Luque, H.E. Garrafa-Gálvez, C.A. García-Maro and C.A. Soto-Robles, Study of the optical properties of ZnO semiconductor nanoparticles using Origanum vulgare and its effect in Rhodamine B degradation. Optik, 258, 168937, 2022. https://doi.org/10.1016/j.ijleo.2022.168937.

[21] V.K. Landge, S.H. Sonawane, M. Sivakumar, S.S. Sonawane, G. Uday Bhaskar Babu and G. Boczkaj, S-scheme heterojunction Bi_2O_3-ZnO/Bentonite clay composite with enhanced photocatalytic performance. Sustainable Energy Technologies and Assessments, 45, 101194, 2021. https://doi.org/10.1016/J.SETA.2021.101194.

[22] N. Yudasari, I.K.H. Dinata, C.J. Shearer, P.H. Blanco-Sanchez, W.P. Tresna Isnaeni, M.M. Suliyanti and H. Trilaksana, Laser-assisted deposition of Ag on self-sourced growth ZnO nanorods as reusable photocatalysts for water purification. Inorganic Chemistry Communications, 146, 110065, 2022. https://doi.org/10.1016/j.inoche.2022.110065.

[23] J. Maalmarugan, R.Z. Ferin, G. Joesna, A. Mustafa, M.G. Mohamed, M. Bououdina, D. Sankar, M. Vimalan and K. SenthilKannan, In situ grown ZnO nanoparticles using Begonia leaves–dielectric, magnetic, filter utility and tribological properties for mechano-electronic applications. Applied Physics A, 128, 217, 2022. https://doi.org/10.1007/s00339-022-05371-w.

[24] H. Oudghiri-Hassani, S. Rakass, F.T. Al Wadaani, K.J. Al-ghamdi, A. Omer, M. Messali and M. Abboudi, Synthesis, characterization and photocatalytic activity of α-Bi_2O_3 nanoparticles. Journal of Taibah University for Science, 9, 508–512, 2018. https://doi.org/10.1016/j.jtusci.2015.01.009.

[25] A. Boumezoued, K. Guergouri, R. Barille, D. Rechem and Z. Mourad, Synthesis and characterization of ZnO-based nano-powders: study of the effect of sintering temperature on the performance of ZnO–Bi_2O_3 varistors. Journal of Materials Science: Materials in Electronics, 32, 3125–3139, 2021. https://doi.org/10.1007/S10854-020-05062 -3.

[26] M. Qayoom and G.N. Dar, Crystallite Size and Compressive Lattice Strain in $NiFe_2O_4$ Nanoparticles as Calculated in Terms of Various Models: Influence of Annealing Temperature. International Journal of Self-Propagating High-Temperature Synthesis, 29, 213–219, 2020. https://doi.org/10.3103/S1061386220040111.

[27] L. Zhou, Z. Han, G.D. Li and Z. Zhao, Template-free synthesis and photocatalytic activity of hierarchical hollow ZnO microspheres composed of radially aligned nanorods. Journal of Physics and Chemistry of Solids, 148, 109719, 2021. https://doi.org/10.1016/j.jpcs.2020.109719.

[28] D.T.C. Nguyen, H.T.N. Le, T.T. Nguyen, T.T.T. Nguyen, L.G. Bach, T.D. Nguyen and T.V. Tran, Multifunctional ZnO nanoparticles bio-fabricated from Canna indica L. flowers for seed germination, adsorption, and photocatalytic degradation of organic dyes. Journal of Hazardous Materials, 420, 126586, 2021. https://doi.org/10.1016/j.jhazmat.2021.126586.

[29] J. Ridwan, J. Yunas, A.A. Umar and A.A. Mohd Raub, Hydrothermal Grow of Cu doped ZnO Nanorods for Large Spectrum Photocatalyst. 2021 IEEE Regional Symposium on Micro and Nanoelectronics, 108–111, 2021. https://doi.org/10.1109/RSM52397.2021.9511572.

[30] R. Kalia, Pushpendra, R.K. Kunchala, S.N. Achary and B.S. Naidu, New insights on photocatalytic hydrogen evolution of $ZnFe_2{-}xGa_xO_4$ ($0 \leq x \leq 2$) solid solutions: Role of oxygen vacancy and ZnO segregated phase. Journal of Alloys Compounds, 875, 159905, 2021. https://doi.org/10.1016/j.jallcom.2021.159905.

[31] K. Lefatshe, C.M. Muiva and L.P. Kebaabetswe, Extraction of nanocellulose and in-situ casting of ZnO/cellulose nanocomposite with enhanced photocatalytic and antibacterial activity. Carbohydrate Polymers, 164, 301–308, 2017. https://doi.org/10.1016/j.carbpol.2017.02.020.

[32] M.A. Abu-Dalo, S.A. Al-Rosan and B.A. Albiss, Photocatalytic, Photocatalytic Degradation of Methylene Blue Using Polymeric Membranes Based on Cellulose Acetate Impregnated with ZnO Nanostructures. Polymers, 13, 3451, 2021. https://doi.org/10.3390/polym13193451.

[33] Y.J. Shim, V. Soshnikova, G. Anandapadmanaban, R. Mathiyalagan, Z.E.J. Perez, J. Markus, Y. Ju Kim, V. Castro-Aceituno and D.C. Yang, Zinc oxide nanoparticles synthesized by Suaeda japonica Makino and their photocatalytic degradation of methylene blue. Optik, 182, 1015–1020, 2019. https://doi.org/10.1016/j.ijleo.2018.11.144.

[34] M. N. M. Nor and M. Shamsuddin, Biosynthesis of zinc oxide nanoparticles using Ficus Auriculata (elephant ear fig) leaf extract and their photocatalytic activity. eProceedings Chemistry, 1, 79–83, 2016.

[35] T. Varadavenkatesan, E. Lyubchik, S. Pai, A. Pugazhendhi, R. Vinayagam and R. Selvaraj, Photocatalytic degradation of Rhodamine B by zinc oxide nanoparticles synthesized using the leaf extract of Cyanometra ramiflora. Journal of Photochemistry Photobiology B: Biology, 199, 111621, 2019. https://doi.org/10.1016/j.photobiol.2019.111621.

[36] M.A. Al-Bedairy and H.A.H. Alshamsi, Environmentally Friendly Preparation of Zinc Oxide, Study Catalytic Performance of Photodegradation by Sunlight for Rhodamine B Dye. Eurasian Journal of Analytical Chemistry, 13, 72, 2018. https://doi.org/10.29333/ejac/101785.

[37] H.A. Alshamsi and A.A. Jaffer, New Hibiscus Sabdariffa L petals extract based Green synthesis of zinc oxide nanoparticles for photocatalytic degradation of Rhodamine B dye under solar light. AIP Conference Proceedings, 2394, 040017, 2022. https://doi.org/10.1063/5.0121228.

[38] H. Li, J. Liu, C. Wang, H. Yang and X. Xue, Oxygen vacancies-enriched and porous hierarchical structures of ZnO microspheres with improved photocatalytic performance. Vacuum, 199, 110891, 2022. https://doi.org/10.1016/j.vacuum.2022.110891.

[39] S. Wang, P. Kuang, B. Cheng, J. Yu and C. Jiang, ZnO hierarchical microsphere for enhanced photocatalytic activity. Journal of Alloys Compounds, 741, 622–632, 2018. https://doi.org/10.1016/j.jallcom.2018.01.141.

[40] A. Lei, B. Qu, W. Zhou, Y. Wang, Q. Zhang and B. Zou, Facile synthesis and enhanced photocatalytic activity of hierarchical porous ZnO microspheres. Materials Letters, 66, 72–75, 2012. https://doi.org/10.1016/j.matlet.2011.08.011.

[41] Y. Su, J. Li, Z. Luo, B. Lu and P. Li, Microstructure, growth process and enhanced photocatalytic activity of flower-like ZnO particles. RSC Advances, 6, 7403–7408, 2016. https://doi.org/10.1039/C5RA24492G.

[42] E. M. Samsudin, S. N. Goh, T.W. Yeong, T. T. Ling, S. B. Abd Hamid and J. C. Juan, Evaluation on the Photocatalytic Degradation Activity of Reactive Blue 4 using Pure Anatase Nano-TiO_2. Sains Malaysiana, 44, 1011–1019, 2015.